Engineering Geology 201 (2016) 45–56

Contents lists available at ScienceDirect

Engineering Geology

journal homepage: www.elsevier.com/locate/enggeo

Wave propagations through jointed rock masses and their effects on the stability of slopes

Ailan Che *, Hongkai Yang, Bin Wang, Xiurun Ge

School of Naval Architecture, Ocean and Civil Engineering, Shanghai Jiao Tong University, Shanghai 200030, China

ARTICLE INFO

Article history:
Received 22 June 2015
Received in revised form 14 December 2015
Accepted 19 December 2015
Available online 23 December 2015

Keywords:
Rock slope
Wave propagation
Discontinuity
Shaking table tests
Seismic stability

ABSTRACT

Seismic behavior in rock slopes with discontinuities is largely governed by the geometrical distribution and mechanical properties of the discontinuities. Particularly, high and steep rock slopes, which are dominated by bedding and toppling discontinuity joints, are likely to collapse and cause serious damage to structures near the slopes. Because the composition of geological materials and discontinuities becomes more complex, and depending on the specifics of the ground motion caused by the earthquake, slope stability becomes very complicated under earthquake loadings. Special attention should be paid to the study of wave propagation phenomena in rock masses and their effects on the stability of rock mass slopes. This research first focuses on the analysis of the wave propagation phenomenon using numerical methods. The wave propagation characteristics in rock mass slopes with bedding and toppling discontinuity joints are assessed using two-dimensional, dynamic FEM analyses. An analytical result is obtained in the time domain and allows one to consider multiple wave reflections between joints. Next, a series of shaking table tests are conducted on a scaled model of a high and steep rock slope with bedding discontinuity joints. The shaking table tests are performed to evaluate the influence of wave propagation on the stability of the slope. These tests show that an amplification area will form at the top of the slope. When the amplitude of the input acceleration reaches a certain value, an area at the top of the slope completely collapses along a slide surface, which is simulated using Teflon tape in the experiments.

1. Introduction

An 8.0 Ms Wenchuan earthquake occurred on May 12, 2008, in the Sichuan province of central China. The epicenter is close to the Longmen Mountain region. This earthquake not only caused extensive damage to rural houses, educational and health care facilities, and lifeline engineering systems but also induced an abundance of landslides and other geologic disasters, such as collapses, debris flow, and shattered mountains (Li and He, 2009). In the field surveys of geological disasters after the earthquake, we observed that several large stones on a peak of Shizi Hill in Qingchuan County near the epicenter of Wenchuan were moved and rotated after the main shock. This indicated that the vertical acceleration at the peak was very strong, exceeding 1000 gal (Xu and Huang, 2008). In general, rock masses on slopes are collapsed by P- and S-waves. First, rock masses on the slopes are shaken vertically and lateral cracks are induced on the slope surface by P-waves. This weakens the rocks and slope stability. Second, landslides and collapses are induced by the strong horizontal shaking from S-waves. Field investigations in the damaged areas showed that the fractured surfaces of landslides are characterized by rough and serrate shapes. These features are quite different from those of non-earthquake-induced landslides, which have smooth, curved surfaces. It is generally considered that rough and serrated fracture surfaces are formed by earthquakes. Fig. 1 shows, a nearly vertical back edge with a rough and serrated fracture plane (Yin, 2009) at the landslide in the village of Dongjia in Qingchuan County. Most of the landslides near the epicenter of the Wenchuan earthquake were subjected to strong lateral S-wave forces and were characterized by “throw-like collapses”. Given the phenomena that drive the slide body, there is an area where the original geomorphology does not change and ground vegetation does not have any relicts. In this case, the slide body can be considered to be “thrown out” with certain acceleration by the S-waves, and the thrown area is called the “slide-out area” (Fig. 2). Around large sliding bodies, numerous heavy stones (tens to hundreds of tons) have been thrown away by tens to hundreds of meters because of the earthquake. We can see such throwing stones in the town of Yingxiu, which was the epicenter of the earthquake. A heavy stone (~300 t) was thrown out from the top of a steep cliff over a highway to the outside pavement. The horizontal acceleration of the heavy stones was estimated to be approximately 1400 gal based on field observations and a preliminary analysis (Yin, 2008).

Sliding and collapse during earthquakes are the main forms of geological disasters on slopes, and the dynamic stability of slopes has been

* Corresponding author at: Dongchuan road 800, Shanghai 200030, China. Tel.:/Fax. +86 21 34206564.
E-mail address: alche@sjtu.edu.cn (A. Che).

http://dx.doi.org/10.1016/j.enggeo.2015.12.018
0013-7952/

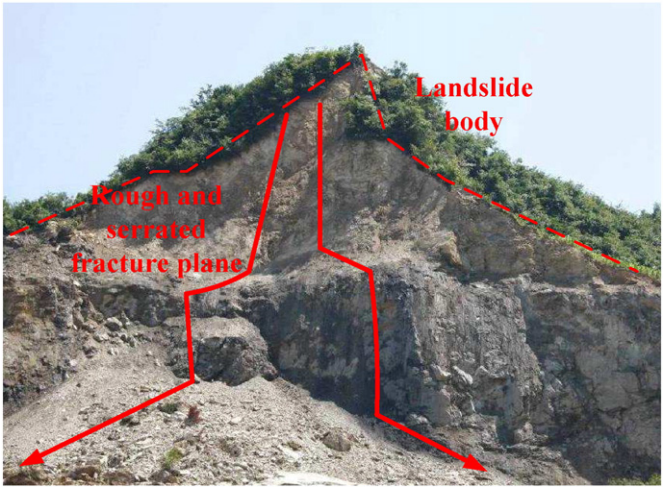

Fig. 1. The landslide at Dongjia village Qingchuan County.

one of the most important topics in geotechnical and seismic engineering. The failure modes of rock slopes predicted by simple models are shown as plane sliding, wedge sliding, toppling or some combinations of these modes (Goodman, 1989). However, given the complexity of the slope compositions and discontinuities in geological materials, and given the nature of earthquake-induced ground motion, it is difficult to quantitatively assess failure potentials (Hudson and Harrison, 1997; He and Liu, 1998; Kumsar et al., 2000). It is well known that rock joints and discontinuities play an important role in wave propagations (Crampin, 1984; Schoenberg and Douma, 1988). Wave propagation in rock masses and its influence on slope stability have become some of the most important topics in rock dynamics and earthquake engineering.

The propagation of seismic waves in jointed rock masses can be modeled by assuming the medium to be continuous or discontinuous. Many numerical methods are available for studying rock engineering issues. These methods are very useful for solving more complex but realistic problems that could not be solved using traditional approaches. Additionally, there are both continuous and discontinuous; medium numerical methods to analyze the wave propagation and seismic stability of rock masses. The continuous medium numerical methods include the finite flement method (FEM) (Goodman et al., 1968; Pande et al., 1990; Matsui and San, 1992; Schwer and Lindberg, 1992), the finite difference method (FDM) (Schwer and Lindberg, 1992) and the boundary element method (BEM) (Crotty and Wardle, 1985) and their combined methods (Beer, 1986). These methods consider discontinuities such as faults, joints, and cracks in the rocks as special joints elements. The discrete element method (DEM) is a useful discontinuous medium numerical method (Cundall, 1971), that models the rock mass as an assemblage of rigid or variable blocks cut by faults, joints and cracks interacting with one another. Discontinuous deformation analysis (DDA) is a type of discrete element method originally proposed by Shi, 1988. DDA adopts a stepwise approach to solve for the large displacements that accompany discontinuous movements between blocks; it is capable of simulating discontinuous problems like jointed rock slopes (Shi and Goodman, 1988). The numerical manifold method (NMM) and meshless method offer the possibility of a discretized approach without the entanglement of the mesh (Zhu et al., 2011; Zhuang et al., 2014a, 2014b). There are remarkable successes reported in applying these methods for analyzing challenging engineering problems (Zheng et al., 2014; Zhuang et al., 2014c). To model rock fractures, Ngo and Scordelis (1967) proposed a two-node linkage element to represent a rock joint. As an improvement, based on the lumped interface, Goodman et al. (1968), Goodman, (1976) proposed a joint element for the FEM. The Goodman joint element is a linear line element suitable for 2D analysis with four nodes and no thickness. The stiffness matrix for the joint element is derived in the same way as that for the regular finite element method. Mehtab and Goodman (1970) extended the formulation of the Goodman joint element to a 3-D solution.

The problem of wave propagation in discontinuous media has been studied by many authors (Achenbach and Li, 1986a, 1986b; Roy and Pyrak-Nolte, 1995) but the analysis of the effects of multiple reflections between the joints has not been widely discussed. Moreover, the influence of the dynamic loads on the rock mass slope has not been extensively investigated either. Given these facts, a better understanding of wave propagations in rock masses and their effects on the stability of the rock mass slope are needed.

In order to clarify the effects of the discontinuity joints on the wave propagation characteristics in rock mass slopes, two-dimensional dynamic FEM analyses with bedding, toppling joints and its combined distribution are performed. The dynamic response of the acceleration is studied, and the response in the time domain and peak ground acceleration are assessed. To evaluate the influence of wave propagation on the stability of the slope, a series of shaking table tests are conducted on a scaled model of a high and steep rock slope with bedding discontinuity joints. Teflon tape is used to simulate the discontinuity joint. The dynamic response of the acceleration compared with simulation results and failure mechanism is discussed.

2. Wave propagation characteristics of the rock mass slope with joints

FEM dynamic analyses were performed for wave propagations through rock masses with joints in two-dimensions. Abaqus/Explicit is chosen as the solver for its transient dynamics simulation capabilities (Abaqus Explicit User Manual). For effectively simulating wave propagations in a discontinuous medium, the size, degree of subdivision and

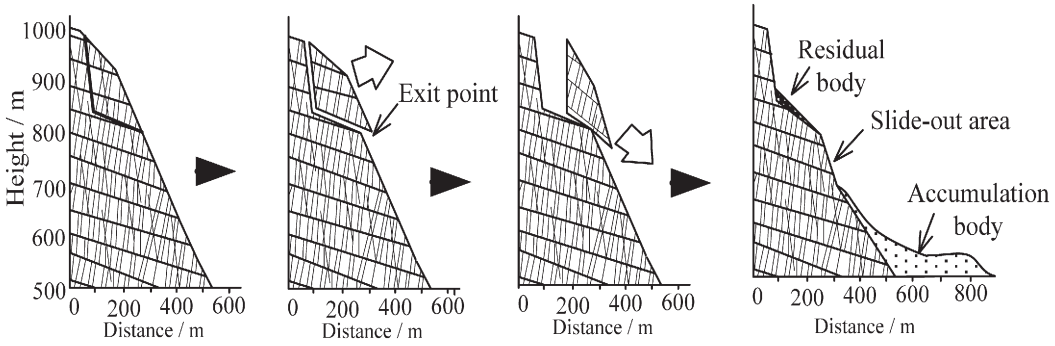

Fig. 2. Evolution process of landslide under the earthquake motions.

boundary conditions of the FEM models need to be optimized (Li et al., 2014; Rabczuk and Areias, 2006). When an elastic wave impinges on a joint, part of the energy is transmitted, and part of it is reflected, refracted and converted. The amplitudes of the transmitted and reflected waves depend on the joint model, its geometrical properties (spacing, length, thickness) and the frequency content of the wave. These joints can be modeled with a linear elastic behavior or more complex models with dissipative behavior. Here, the joints are simulated as a soft material rigidly connected to the surrounding rock mass and are considered to be large in extent and small in thickness compared to the wavelength. When the reflection coefficient between the interface of the joint and rock mass is large, multiple wave reflections are considered. The principal effects of the rock joints on wave propagation are the attenuation and slowdown of the incident wave. Considering the reflection and scattering of the seismic wave in the boundary, the infinite element boundary condition is used at both sides and the base of the model. The infinite element is combined with the finite element. Inputting the seismic wave at the nodes of the finite element at the bottom of model, the dynamic response in near field region is simulated by the finite element, and that in the far field region is simulated by the infinite element. Because the reflection and scattering of the seismic wave in the boundary can be directly absorbed by infinite elements, the high frequency noise is considered to be removed and does not affect the effective periodic component of the stress wave near the sliding surface.

To clarify the effects of the discontinuity joints distribution on wave propagation, 4 types of slopes with regularly distributed discontinuity joints were modeled, which are case 1: without joints, case 2: with ordered bedding joints, case 3: with ordered toppling joints and case 4: with disordered joints, as shown in Fig. 3. The slope was 90 cm high with a gradient of approximately 60°. The discontinuity joints were set in 10 cm intervals approximately 8 cm in length, 1 cm in width and a 40° (bedding) or 140° (toppling) gradient in the rock slope. Plane strain elements were used to simulate the rock mass and discontinuity joints. Infinite element boundaries were set on edge of the model to simulate semi-infinite ground conditions, while the propagation was approximately expressed by the viscous damping using dash pots. Meshes of quadrilaterals and squares with a side length of 0.01 m were used to explore some of the qualitative features of the behavior in the model. Next, 21,654 plane strain elements were generated in the finite element model. The assumed mechanical properties of the rock mass are listed in Table 1; the materials are considered as elastic.

Table 1
Mechanical parameters of media in the model.

Physical variable	Density ρ/kN/m^3	Poisson ratio μ	Dynamic elastic modulus E/GPa
Rock	24.8	0.24	0.98
Joint	11.0	0.45	0.0001

Ricker wavelets are often used as an artificial excitation force in the dynamic simulation analysis and are characterized by a simple functional excitation force concentrated in short duration (Longman, 1980). Conversely, the contained frequency components can be concentrated in a frequency band around a certain frequency. To satisfy the requirement that there be no less than a twentieth wavelength in each mesh, the frequency of the input motion was selected as 500 Hz, according to the parameters of the material. A Ricker wavelet of unit amplitude (1 gal) was applied at the bottom boundary of the model with a frequency of $f = 500$ Hz, $t = 0.05$ s and $\Delta t = 1.0 \times 10^{-4}$ s to create time-dependent acceleration inputs at the bottom of the slope during horizontal and vertical motions in the calculations.

Fig. 4 shows the acceleration results based on calculations without considering the initial stress due to gravity. The numbers of the plots refer to the points on the slope shown in Fig. 3. The calculation considers the horizontal and vertical input motions. Compared with the response of the 4 models, the acceleration history on the surface of and inside the slope shows that the accelerations are clearly amplified along the slope surface, reaches its maximum at the top of the slope, and then decreases along the top surface of the model. The accelerations inside the slope show almost no amplification in both cases of horizontal and vertical

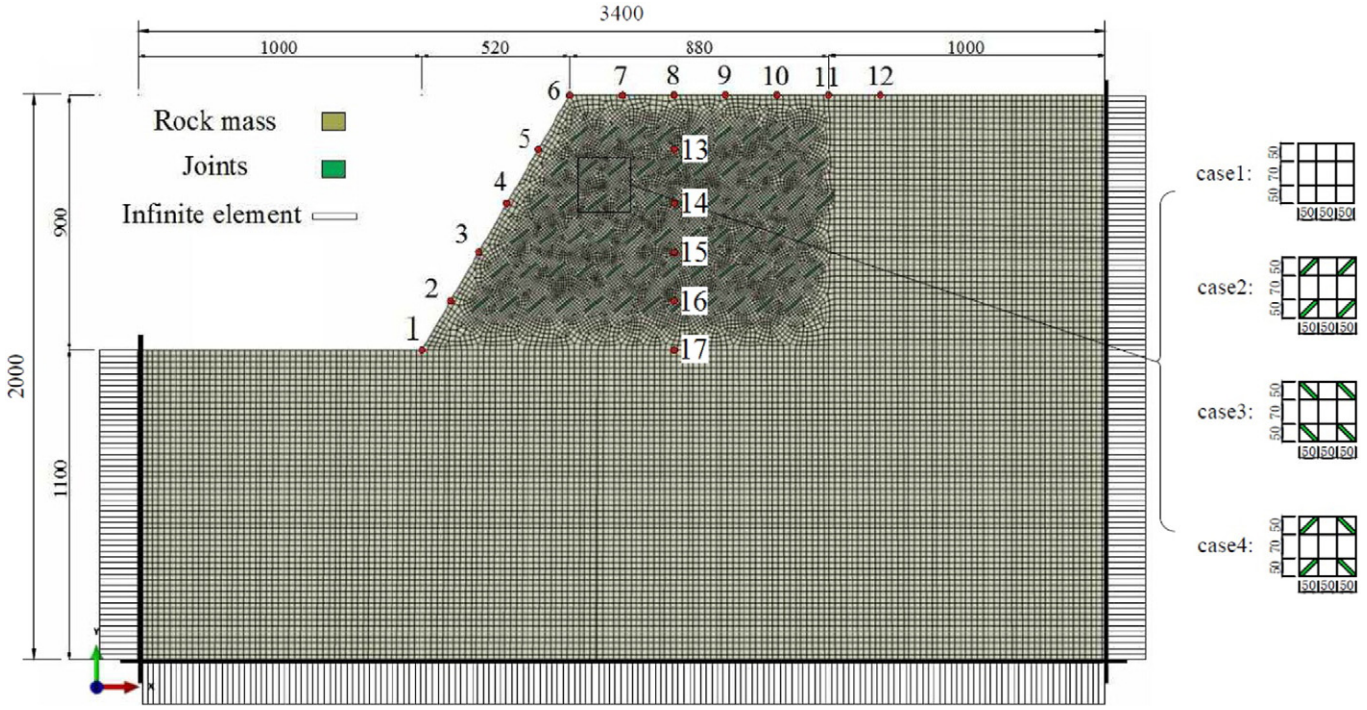

Fig. 3. Mesh model used in the calculations.

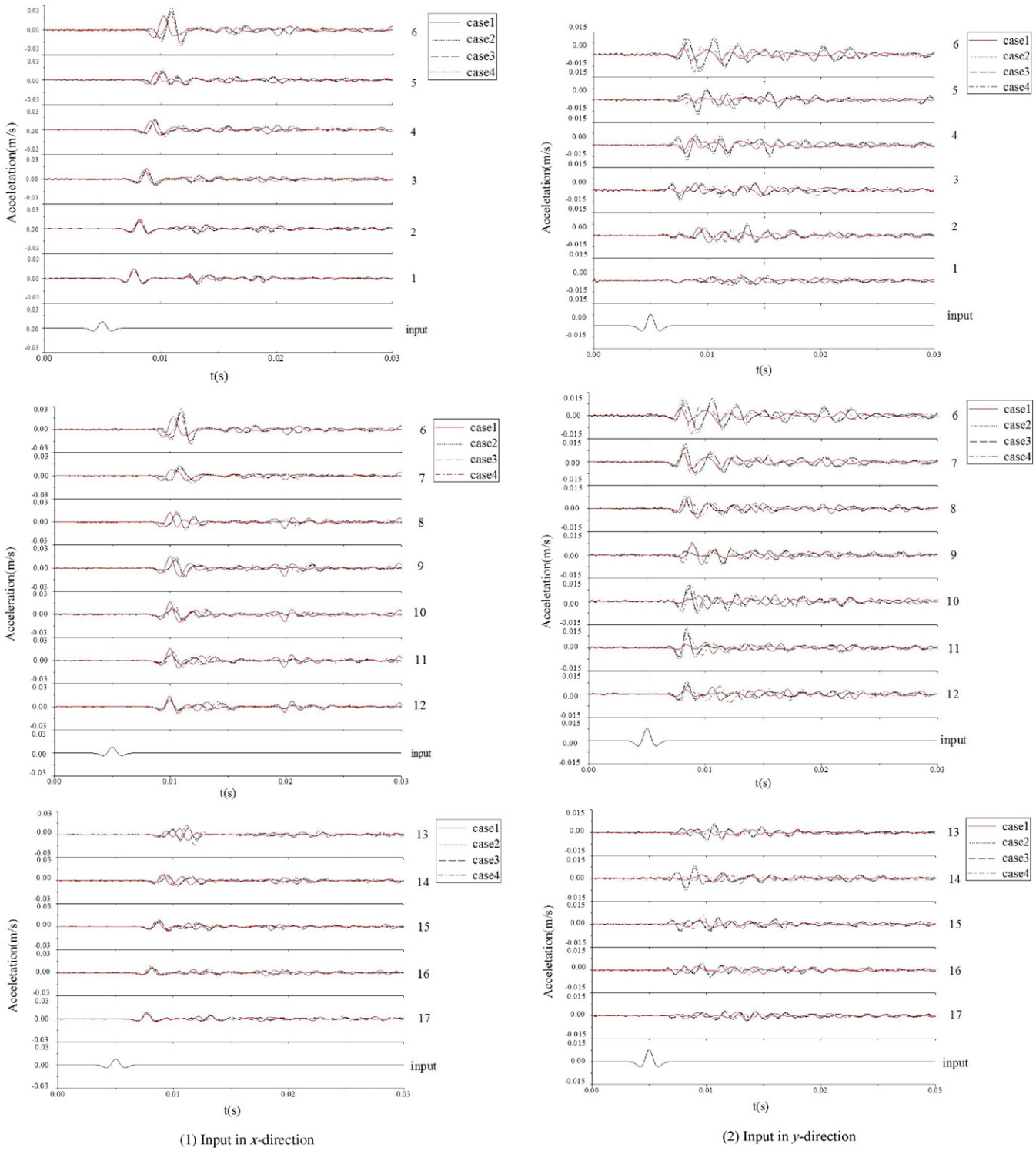

Fig. 4. Time–history curves of accelerations.

input motions. Therefore, an amplified area at the top of the slope, where the mechanical properties are very unstable, will form. The joints in the slope model may slow down and amplify the effects on wave propagation, especially in the horizontal input motions. The time delay and amplification are related with the joint number and distribution of the joints, and the phase shift and acceleration reaches maximum at the tip of the slope. The wave propagation characteristics are quite different between the horizontal and vertical input motions. The shear wave propagation is predominant in the horizontal input motion, and it shows surface wave propagation in the vertical input motion. Moreover, the phase shift, θ, is significant for shear waves.

The amplification coefficient of the peak ground acceleration (PGA) is defined as the ratio of the PGA of the transmitted wave to that of the incident wave. Fig. 5 shows the distribution of the amplification coefficient of the PGA for the 4 models. It is clearly shown that an

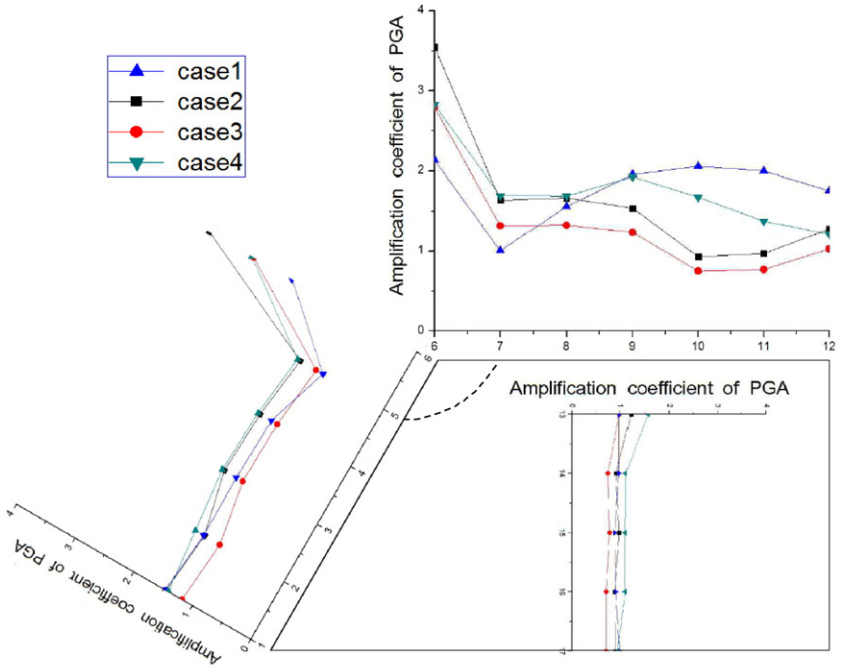

(1) Input in *x*-direction

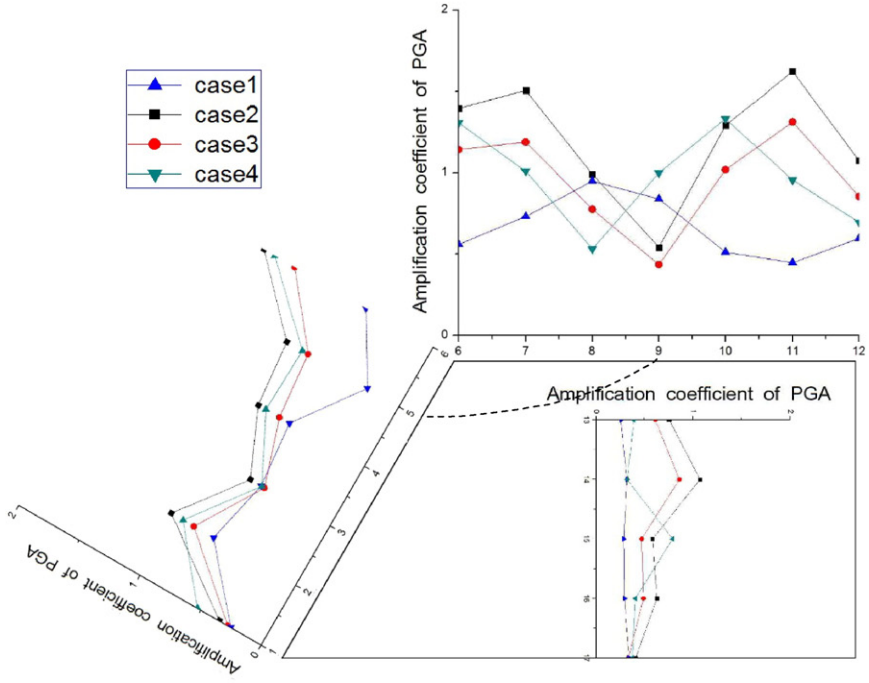

(2) Input in *y*-direction

Fig. 5. Distribution of the amplification coefficient of PGA.

amplified area formed at the top of the slope, where the mechanical properties are very unstable. The amplified area and unstable property show quite a difference between the horizontal and vertical input motions. The mechanical properties are very unstable in the horizontal input motions and the area is smaller than that in vertical input motions. The joints and its distribution in the slope model have a positive effect on the amplification characteristics. The amplification coefficients at the tip of the slope are 2.13 and 0.56 in case 1; 3.55 and 1.4 in case 2; 2.8 and 1.14 in case 3; and 2.82 and 1.31 in case 4 in the horizontal and vertical directions, respectively. The amplification coefficient appears most in the model with ordered bedding joints in both the horizontal and vertical input motions. It can be assumed that the bedding structure gives rise to unique diffraction/reflection patterns with large amplifications.

3. Shaking table tests for a scale model of a rock mass slope with joints

To reduce the risk of geotechnical engineering structural failures in a slope environment, the seismic stability of the slope has to be the main

Fig. 6. Soil container and scaled model.

goal. The challenges with the shaking table test system are (1) simulation of the rock material and (2) simulation of the discontinuous joints. The test system is composed of a shaking table, a soil container, and a data acquisition system.

3.1. Shaking table

Tests using a bi-directional (horizontal and vertical) electric servo shaking table made by Japan Kokusai Corporation were performed in the Key Laboratory of Loess Earthquake Engineering, Gansu Earthquake Administration. The shaking table is 4 m × 6 m, and utilizes a single, horizontal translation degree of freedom. With a maximum load of 25 t, a maximum horizontal acceleration of 1.7 g and a maximum vertical acceleration of 1.2 g can be reached. Regular and irregular waves can be used as input motions, and the effective frequency range is 0.1 to 70 Hz.

3.2. Soil container

A soil container was developed for the tests. It was designed as a rigid, sealed box with organic glass and carbon steel plates, as shown in Fig. 6. The inside of the box is 2.8 m × 1.4 m × 1.0 m.

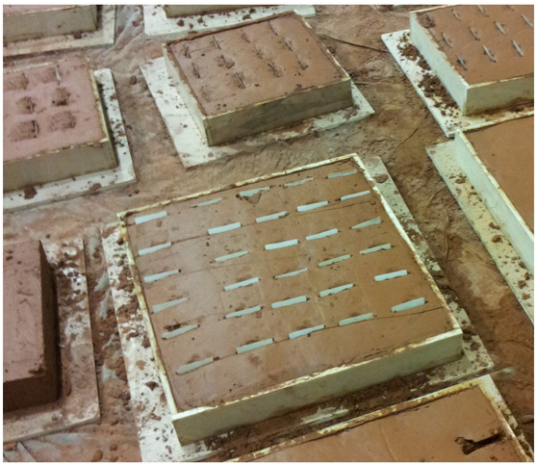

Fig. 7. Prefabricated blocks and Teflon tape.

The law of similitude was adopted to determine the dynamic testing conditions for the models (Xu et al., 2010). The movement of a landslide depends on the shearing resistance of the slope mass, which is mainly characterized by the coefficient of friction. Therefore, it is important to ensure that the materials forming the laboratory model possess are similar engineering properties to that of the actual field slope. The model material was constructed from a cement, sand, iron powder, clay and water mixture, with a gradation of 0.325:11:4:0.8:0.025:2.7, respectively. The parameters of the simulated rock mass materials were obtained from a triaxial test. These parameters were found to be: density of $\rho = 15.5$ (kN/m^3); shear modulus of $G_0 = 98$ MPa; Poisson ratio of $\mu = 0.264$; cohesion of $c = 0.074$ MPa; and a friction angle of $\varphi = 35°$.

3.3. Scaled model

To clarify the seismic stability of the slope, the abstract generalized geological model was simulated. The slope model was 1.0 m tall, 2.8 m in length and 1.4 m wide, with a slope angle of 60°. Prefabricated blocks and Teflon tape were used to simulate the rock mass and discontinuities, respectively, as shown in Fig. 7. Strips of 8-cm-long Teflon tape were spaced 10 cm apart at a 45° angle to simulate discontinuous joints in the model material, as shown in Fig. 8.

3.4. Measurements

The measurement points are shown in Fig. 9. Twenty accelerometers were installed along two measurement directions, denoted as A1–A12. Accelerometers A1, A2, A3, A4, and A5 were placed on the slope surface. Accelerometers A5–A12 were embedded at various depths in the slope. A 3-direction capacitive acceleration sensor (DH301) made by Huadong Testing Co., LTD. was used. The sensitivity of this sensor is -66 mV/ms^2 and its range is ± 20 m/s^2. Additionally, its frequency range is 0–1500 Hz horizontally and 0–800 Hz vertically. The data recorder used was a Yiheng Premax made by Yiheng Co., LTD.; the possible sampling rates are 10, 20, 50, 100, 200, 500, 1 k, 2 k, 5 k, 10 k, and 20 kHz. To minimize the side boundary effect, all of the sensors were embedded into the center of the slope model. The bottom boundary effect was minimized by laying an additional 10-cm-thick buffer layer made of similar materials as the slope at the base of the model.

3.5. Dynamic response during the earthquake test

A series of shaking table tests were performed. For the sine-sweep tests (amplitude of acceleration = 50, 100, 200 and 400 gal, and alternating frequency = 3–50 Hz, as shown in Fig. 10a) and random

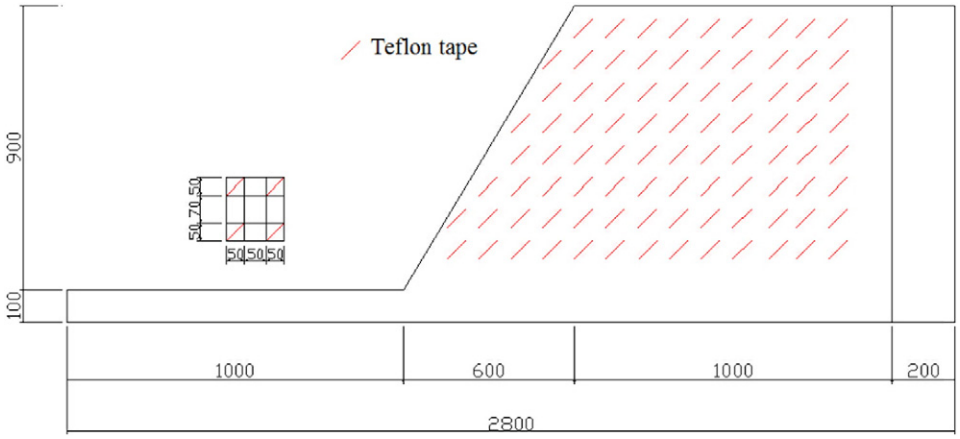

Fig. 8. Slope model.

vibration tests, the recorded horizontal accelerations at the Wenxian Seismic Station, Gansu Province (104.48°N, 32.95°E), during the Wenchuan earthquake (maximum acceleration = 184.9 gal, 10 s after the shaking start, as shown in Fig. 10b), were input in the horizontal, *x*, and vertical, *z*, directions.

Signals recorded from the accelerometers were subjected to undesired noise interferences. It was necessary to perform an appropriate data transformation before the data could be readily used for the subsequent analyses. Pre-filtering, zero-mean normalization, and removal of errors techniques of data transformation were applied. The bandwidth of the frequency was set between 3 and 50 Hz in the pre-filtering process to smooth the response, control the frequencies, and reduce signal noises (particularly high frequency noise from electrical signals) in the data. Blurring in the signals caused by external disturbances or instrument inconsistency was eliminated by the removal of errors.

The peak ground acceleration (PGA) was measured by the twenty acceleration sensors installed in the slope model. To explain deformation phenomena in the slope, the acceleration amplification coefficient of the PGA was adopted to study the dynamic responses of the slope under earthquake loading. The acceleration amplification coefficient in this paper refers to the ratio of the PGA measured within the slope to that measured at the top of the slope. The vertical and horizontal PGA were measured when the vertical (in *z* direction) and horizontal (in *x* direction) seismic waves were loaded, respectively.

Fig. 11 shows the acceleration amplification coefficient distribution of the measurement points during the earthquake. The results show good agreement with the calculation, as shown in Fig. 5. It was found that the acceleration was clearly amplified along the slope surface and reached a maximum at the top of the slope. The amplification coefficient at the tip of the slope reaches

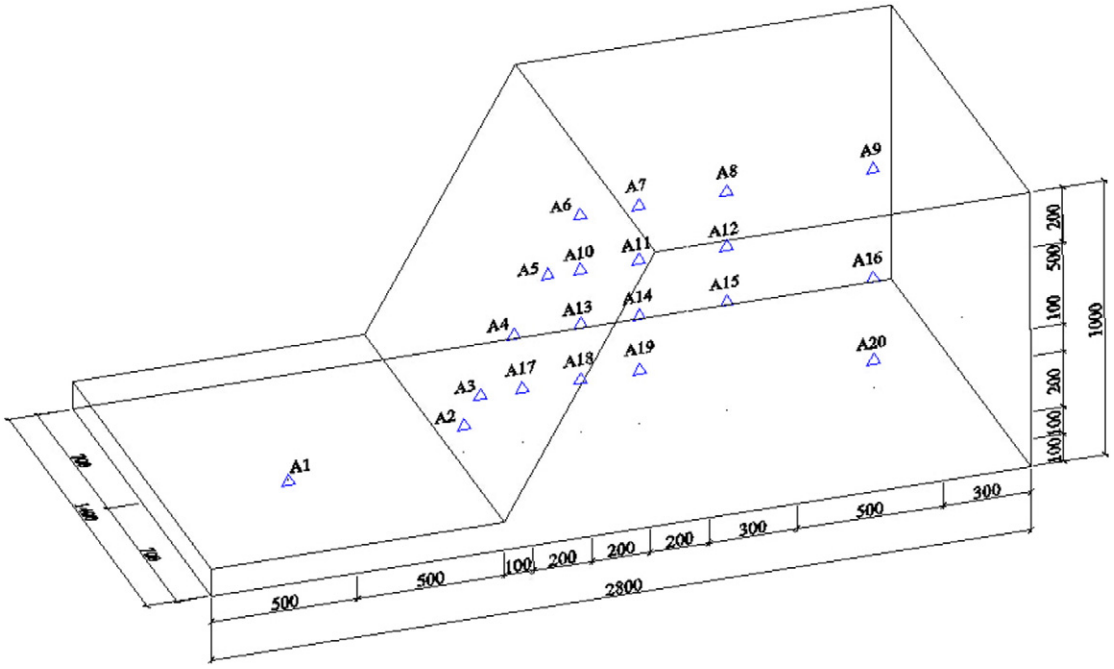

Fig. 9. Layout of measurement points.

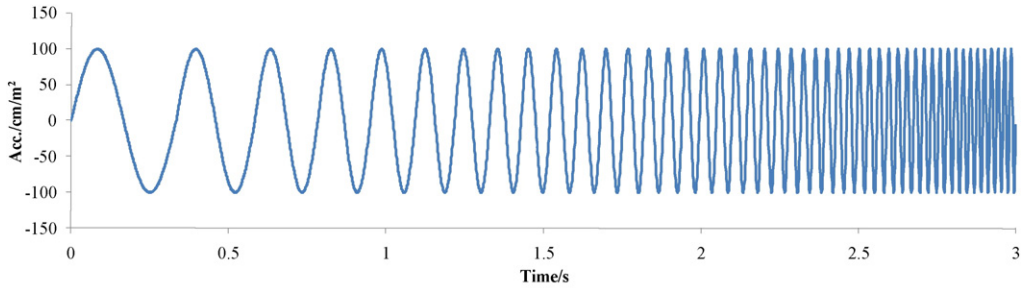

(a) Sine sweep (100 gal)

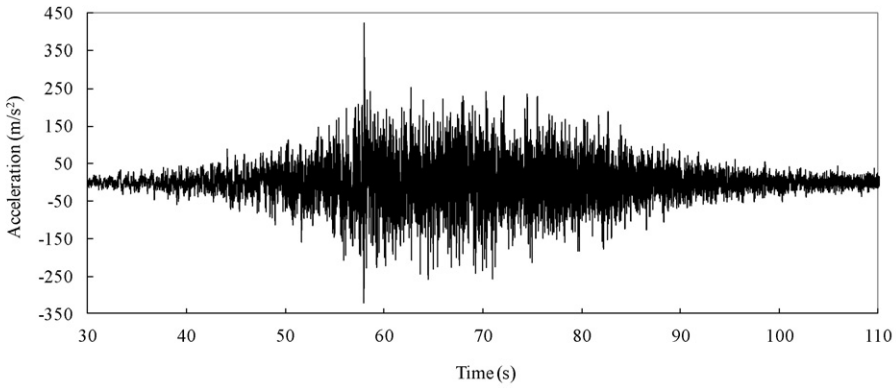

(b) Earthquake records during the Wenchuan great earthquake

Fig. 10. Input motions in shaking table tests.

approximately 3–5 and 2–2.5 in the horizontal and vertical directions, respectively. By comparing the amplification ratios during different input motions, it was observed that the area of the amplification effect expanded upward with increasing acceleration. Therefore, an amplified area at the top of the slope, the mechanical properties of which are very unstable, will form. A large deformation will be generated at the top of the slope under seismic loadings.

From the shaking table test results, two general conclusions can be drawn regarding the impact of seismic waves on slopes with bedding discontinuity joints. (1) The impact of the horizontal seismic wave is larger than that of vertical seismic wave and (2) the impact of seismic waves on the rock slope is generally limited to a shallow depth at the upper part of the slope.

3.6. Failure mechanism

Huang et al. observed that the slope failure mechanism in various models was similar (Huang et al., 2013). The failure of a slope is mainly characterized by the following three notable features. First, the initial sign of the rupture follows the crack near the top surface when the input acceleration exceeds a certain value. The closer to the slope the rupture is, the larger the crack on the top surface is. Second, with an increase in the input acceleration, a collapse occurs on the slope surface, but no sliding body is formed. When the input acceleration continues to increase, the cracks extend and tend to connect. Third, when the input acceleration amplitude reaches a certain value, the top area of the slope completely collapses along a slide surface, which was observed along the setting of the Teflon tape. An obvious slip bond can be drawn in the collapse mechanism, as shown in Fig. 12.

The deformations of the rock slope are shown in Fig. 13. Many vertical fresh fractures in the rock mass are observed in the region higher than 1/3 of slope height from the ground. A small number of horizontal fresh fractures developed along the bends in the slope and formed distinct downward dislocations at the crest of the slope. The failure surface is in a flat and regular shape. From the observations, it can be concluded that the deformations induced by the earthquake mainly occurred at the upper part of the slope. Numerous fresh fractures were formed in the rock mass along the discontinuity joints, resulting in cataclysmic structures.

4. Conclusions

4.1. The wave propagation characteristics of the rock mass slope with bedding and toppling discontinuity joints were assessed by means of dynamic FEM analyses in two dimensions. The following observations can be made

The accelerations increased along the slope, especially at the top of the slope. The amplification coefficient appears most in the model with ordered bedding joints in both the horizontal and vertical input motions, which was 3.5 in the horizontal direction and 1.4 in the vertical direction. It can be assumed that the bedding structure gives rise to unique diffraction/reflection patterns with large amplifications.

The time delay of the transmitted wave is caused by the joints and medium between the joints. This time delay is related

to the number of joints and the distribution of the joints, and the phase shift reaches maximum at the tip of the slope. The shear wave propagation is predominant in the horizontal input motion, and it shows surface wave propagation in the vertical input motion. Moreover, the phase shift, θ, is significant for shear waves.

4.2. A series of shaking table tests was carried out to study the stability of the rock mass slope

The shaking table tests successfully described the deformation phenomena of the earthquake-induced landslides. The deformation of the rock slope mainly developed within a shallow depth in the

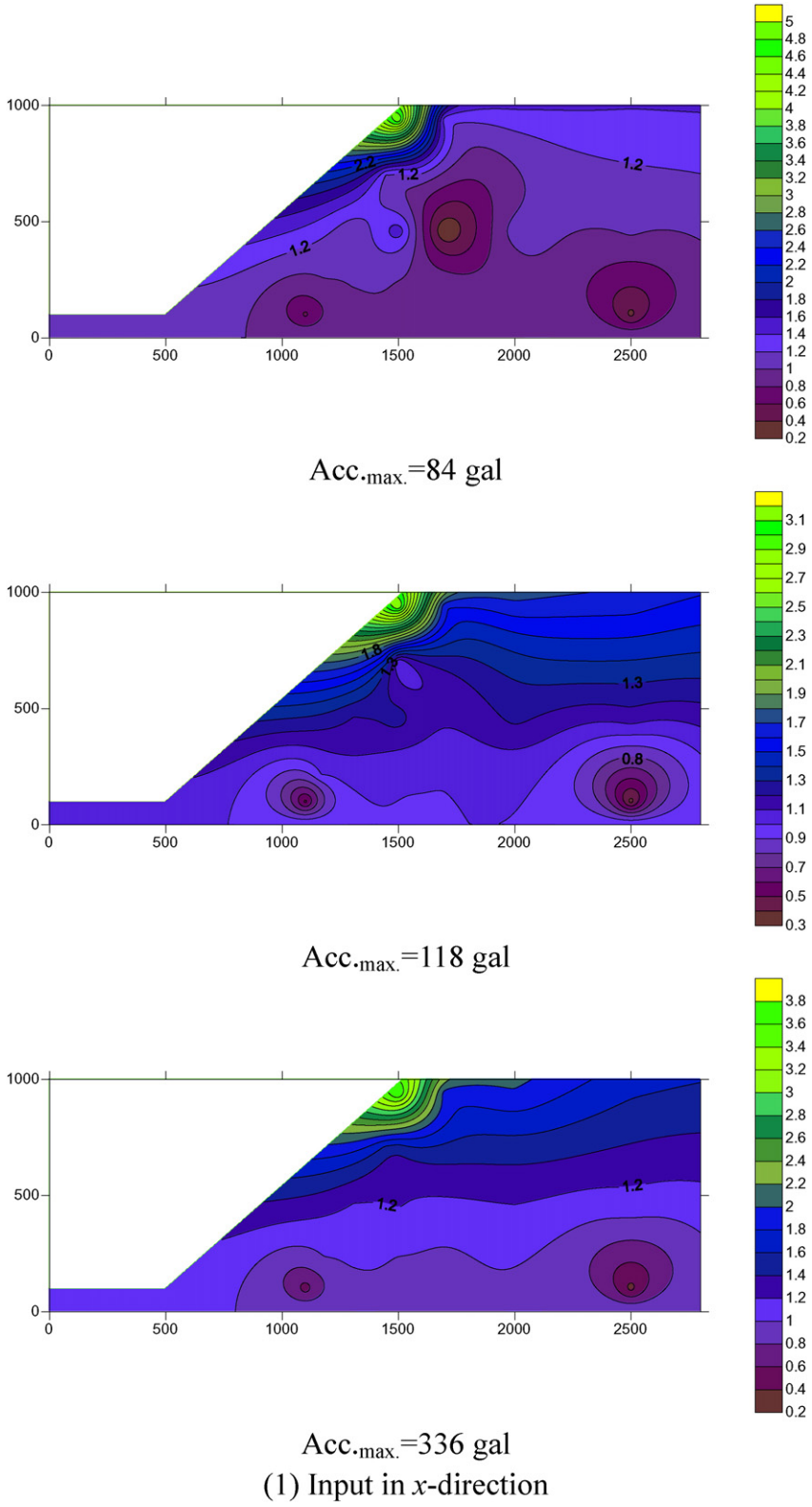

Fig. 11. Acceleration amplification coefficient distribution during Wenchuan earthquake.

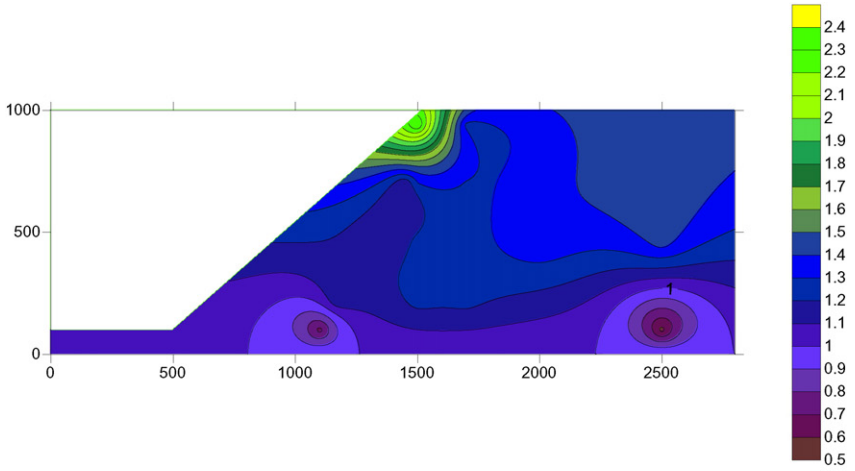

Acc.$_{max.}$=84 gal

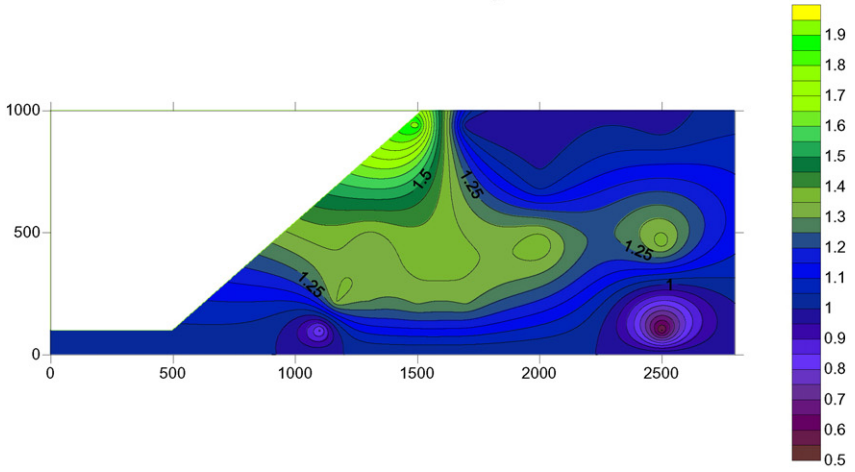

Acc.$_{max.}$=118 gal

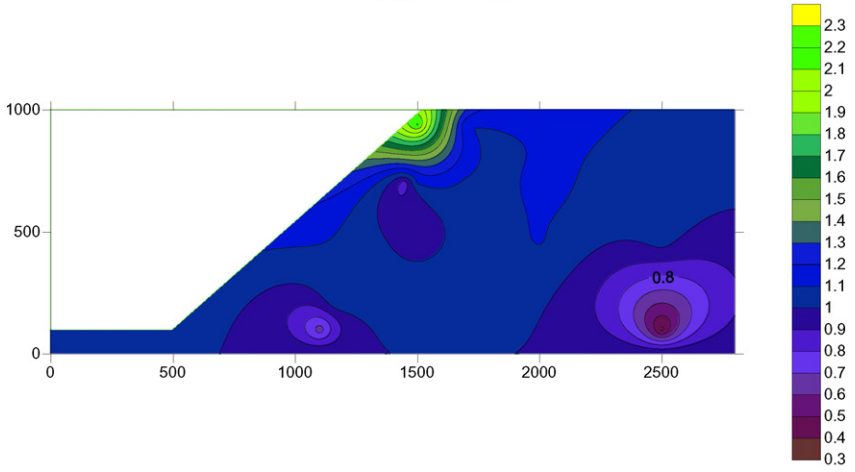

Acc.$_{max.}$=336 gal

(2) Input in *y*-direction

Fig. 11 (*continued*).

upper part of the slope. When the input acceleration amplitude reaches a certain value, the top area of the slope completely collapsed along a slide surface, which was observed along the Teflon tape setting.

The location of the sliding plane in the model is consistent with the location of the maximum horizontal acceleration. An amplified area at the top of the slope, the mechanical

Fig. 12. Photograph of model after shaking.

properties of which are very unstable, will form. A large deformation at the top of the slope will be generated under seismic loadings.

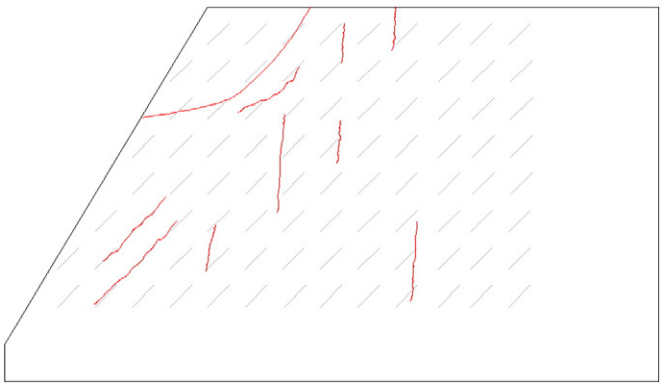

Fig. 13. Deformation characteristics of the slope.

Acknowledgments

This work is supported by the National Basic Research Program (973) of China (No. 2011CB013505) and the National Natural Science Foundation of China (No. 11372180). The authors would like to express their gratitude to Professor Takahiro Iwatate of the Tokyo Metropolitan University for their helpful advice.

References

Achenbach, J.D., Li, Z.L., 1986a. Reflection and transmission of scalar waves by a periodic array of screens. Wave Motion 8, 225–234.
Achenbach, J.D., Li, Z.L., 1986b. Propagation of horizontally polarized transverse waves in a solid with a periodic distribution of cracks. Wave Motion 8, 371–379.
Beer, G., 1986. Implementation of combined boundary element-finite element analysis with applications in geomechanics. Dev. Bound. Elem. Methods 4, 191–225.
Crampin, S., 1984. Effective anisotropic elastic constants for wave propagation through cracked solids. Geophys. J. R. Astron. Soc. 76, 135–142.
Crotty, J.M., Wardle, L.J., 1985. Boundary integral analysis of piecewise homogeneous media with structural discontinuities. Int. J. Rock Mech. Min. Sci. 22 (6), 419–427.
Cundall, P.A., 1971. A computer model for simulating progressive large scale movements in blocky rock systems. Proceedings of the Symposium of the International Society of Rock Mechanics Vol. 1. Nancy, France, pp. 129–136.

Goodman, R.E., 1976. Methods of Geological Engineering in Discontinuous Rocks. first ed. West, New York (472 pp.).
Goodman, R.E., 1989. Introduction to Rock Mechanics. second ed. Wiley, New York.
Goodman, R.E., Taylor, R.L., Brekke, T.A., 1968. A mode of the mechanics of jointed rock. J. Soil Mech. Found. Div. ASCE 94 (SM 3), 637–659.
He, W.L., Liu, S.Y., 1998. Seismic approximation method of rock slope. J. Geotech. Eng. 20 (2), 66–68.
Huang, R.Q., Zhao, J.J., Ju, N.P., Li, G., Lee, M., Li, Y.R., 2013. Analysis of an anti-dip landslide triggered by the 2008 Wenchuan earthquake in China. Nat. Hazards 68, 1021–1039.
Hudson, J.A., Harrison, J.P., 1997. Engineering rock mechanics. An Introduction to the Principles. Pergamon Press, Oxford.
Kumsar, H., Aydan, Ö., Ulusay, R., 2000. Dynamic and static stability assessment of rock slopes against wedge failures. Rock Mech. Rock. Eng. 33 (1), 31–51.
Li, X.J., Zuo, Y.L., Zhuang, X.Y., Zhu, H.H., 2014. Estimation of fracture trace length distributions using probability weighted moments and L-moments. Eng. Geol. 168, 69–85.
Li, X.P., He, S.M., 2009. Seismically induced slope instabilities and the corresponding treatments: the case of a road in the Wenchuan Earthquake hit region. J. Mt. Sci. 6 (1), 90–100.
Longman, I.M., 1980. The calculation of Ricker seismic wavelet functions. Geophysics 45 (6), 1055–1060.
Matsui, T., San, K.C., 1992. Finite element slope stability analysis by shear strength reduction technique. Soils Found. 32 (1), 59–70.
Mehtab, M.A., Goodman, R.E., 1970. Three-dimensional finite element analysis of jointed rock slopes. Proceedings of the 2nd International Congress on Rock Mechanics (Belgrad).
Ngo, D., Scordelis, A.C., 1967. Finite element analysis of reinforcement concrete. Jul. Am. Concr. Inst. 64 (14), 152–163.
Pande, G., Beer, G., Williams, J., 1990. Numerical Methods in Rock Mechanics. John Wiley and Sons Inc., NewYork.
Rabczuk, T., Areias, P.M.A., 2006. A new approach for modelling slip lines in geological materials with cohesive models. Int. J. Numer. Anal. Methods Eng. 30 (11), 1159–1172.
Roy, S., Pyrak-Nolte, L.J., 1995. Interface waves propagating along tensile fractures in dolomite. Geophys. Res. Lett. 22 (20), 2773–2777.
Schoenberg, M., Douma, J., 1988. Elastic wave propagation in media with parallel fractures and aligned cracks. Geophys. Prospect. 36, 571–590.
Schwer, L.E., Lindberg, H.E., 1992. A finite element slideline approach for calculating tunnel response in jointed rock. Int. J. Numer. Anal. Methods Geomech. 16 (7), 529–540.
Shi, G. 1988. Discontinuous Deformation Analysis — a new Numerical Model for the Statics and Dynamics of Block Systems. Phd Dissertation, Department of Civil Engineering, University of California at Berkeley, USA.
Shi, G., Goodman, R.E., 1988. Discontinuous deformation analysis, a new method for computing stress, strain and sliding of block system. Proceedings of 29th U.S. Symposium Rock Mechanics, pp. 381–393.
Xu, Q., Huang, R.Q., 2008. Kinetics characteristics of large landslides triggered by May 12th Wenchuan earthquake. J. Eng. Geol. 06, 721–729.
Xu, Q., Liu, H.X., Zou, W., 2010. Large-scale shaking table test study of acceleration dynamic responses characteristics of slopes. Chin. J. Rock Mech. Eng. 12, 2420–2428.
Yin, Y.P., 2008. Researches on the geo-hazards triggered by Wenchuan Earthquake, Sichuan. J. Eng. Geol. 16, 433–443.
Yin, Y.P., 2009. Features of landslides triggered by the Wenchuan Earthquake. J. Eng. Geol. 01, 29–38.
Zheng, W.B., Zhuang, X.Y., Tannant, D.D., Cai, Y.C., Nunoo, S., 2014. Unified continuum/discontinuum modeling framework for slope stability assessment. Eng. Geol. 179, 90–101.
Zhu, H.H., Zhuang, X.Y., Cai, Y.C., 2011. High rock slope stability analysis using the enriched meshless Shepard and least squares method. Int. J. Comput. Methods 8, 209–228.
Zhuang, X.Y., Cai, Y.C., Augarde, C., 2014b. A meshless sub-region radial point interpolation method for accurate calculation of crack tip fields. Theor. Appl. Fract. Mech. 69, 118–125.
Zhuang, X.Y., Huang, R.Q., Liang, C., Rabczuk, T., 2014c. A coupled thermo-hydro-mechanical model of jointed hard rock for compressed air energy storage. Math. Probl. Eng. 2014, article ID: 179169.
Zhuang, X.Y., Zhu, H.H., Augarde, C., 2014a. An improved meshless Shepard and least square method possessing the delta property and requiring no singular weight function. Comput. Mech. 53, 343–357.